ResearchGate

See discussions, stats, and author profiles for this publication at: https://www.researchgate.net/publication/260406900

Modeling and Simulation for Direct Contact Membrane Distillation in Hollow Fiber Modules

Article *in* AIChE Journal · February 2013

DOI: 10.1002/aic.13845

CITATIONS
46

READS
2,441

2 authors:

Salah Salman Ibrahim
University of Technology, Iraq
29 PUBLICATIONS **340** CITATIONS

SEE PROFILE

Qusay Alsalhy
University of Technology-Iraq
166 PUBLICATIONS **2,633** CITATIONS

SEE PROFILE

All content following this page was uploaded by Qusay Alsalhy on 10 December 2017.

The user has requested enhancement of the downloaded file.

Modeling and Simulation for Direct Contact Membrane Distillation in Hollow Fiber Modules

Salah S. Ibrahim and Qusay F. Alsalhy
Dept. of Chemical Engineering, University of Technology, Alsinaa street 52, Baghdad, Iraq

DOI 10.1002/aic.13845
Published online June 1, 2012 in Wiley Online Library (wileyonlinelibrary.com).

Direct contact membrane distillation (DCMD) offers an attractive operation for the separation of mixtures at atmospheric pressure with reasonable energy requirement. A new simultaneous heat and mass transfer model in DCMD in a hollow fiber configuration is presented. Flow regime in feed and permeate side, the variations of mean temperature and concentration along the membrane module, the length of the membrane, and various properties of membrane characteristics are taken into account in the present model. A system of nonlinear equations describing the DCMD process is solved numerically for each cell using the FSOLVE coding, which is a built-in function in MATLAB® to find the influence of the temperature and velocity of the feed and permeate streams, and the salt concentration of the feed along the module on the permeate flux. The predicted results by the new model show a good accord with a wide range of various experimental results available in the literature. © 2012 American Institute of Chemical Engineers *AIChE J,* 59: 589–603, 2013
Keywords: membrane separation, DCMD, mathematical modeling, desalination

Introduction

The desalination of sea water is commercially performed by reverse osmosis (RO) and thermal processes like multistage flash distillation (MSF). Although such traditional processes are widely used, there is a need for new desalination techniques which are cheaper than both RO and MSF processes or have other significant advantages. Membrane distillation (MD) is considered as a potential alternative to such traditional separation processes.[1]

MD is a novel membrane separation process in which two aqueous solutions at different temperatures are separated by a microporous hydrophobic membrane.[2]

MD is suited for both distilled water production or for the concentration of aqueous solutions. It may offer various advantages in comparison to the traditional distillation and membrane processes if low-grade waste heat energy sources, such as industrial heat streams, geothermic water or even solar energy are provided.[3–6]

MD has been applied for the separation of nonvolatile and trace volatile components from water such as ions, colloids, macromolecules, benzene, chloroform, trichloroethylene, and so forth.[7–12] Moreover, the extraction of alcohols from dilute aqueous solutions has been studied by Garcia-Payo et al.[13] In addition, Tang, et al.[14] also applied MD for the concentration of acids.

However, MD is still being developed at desalination testing stages, and however, it is not fully implemented in industries. The process still under evaluation and different contradicted opinions exist concerning its features.[15]

Correspondence concerning this article should be addressed to Q. F. Alsalhy at qusayalsalhy@yahoo.com or qusayalsalhy@uotechnology.edu.iq.

© 2012 American Institute of Chemical Engineers

There are different configurations developed to perform MD process, one of them considered the most used configuration is the direct contact MD (DCMD). In DCMD, a hot nonvolatile solute containing aqueous solution, such as hot brine, is brought into contact with one side of a porous hydrophobic membrane and a colder aqueous distillate stream flows on the other side of the membrane. Transfer of water vapor from the hot brine at the membrane interface takes place through the hydrophobic membrane pores; the water vapor is condensed in the cold distillate on the other side of the membrane. DCMD is quite attractive, because it operates at atmospheric pressure and it is not subject to the osmotic pressure driven limitations of RO process. For this reason, it can be used to treat brines of various salt concentrations.[1,2,16]

Many attempts appeared in the literature for the modeling of MD process. Almost all of the models apply the fundamental relationships on MD modeling given by Lawson and Lloyd,[17] where permeate flux is determined by considering the heat transfer resistances in all parts and the mass transfer resistance inside the membrane. El-Bourawi et al.[18] presented an extensively revision of numerous modeling studies, with or without experiments, on MD. New papers are still evolving.[19–21] Phattaranawik et al.[22] suggested a model based on the assumption of linear temperature profile through the membrane. This proposed model which was able to study the effect of mass transfer on heat transfer rates and heat transfer coefficients, it covered both flow regimes (laminar and turbulent). Qtaishat et al.[19] used the experimental values of permeate flux to determine the boundary layer's heat transfer coefficients, the membrane heat transfer coefficient, membrane/liquid interface temperatures, and membrane mass transfer coefficient. The deviations of the theoretical and experimental results of

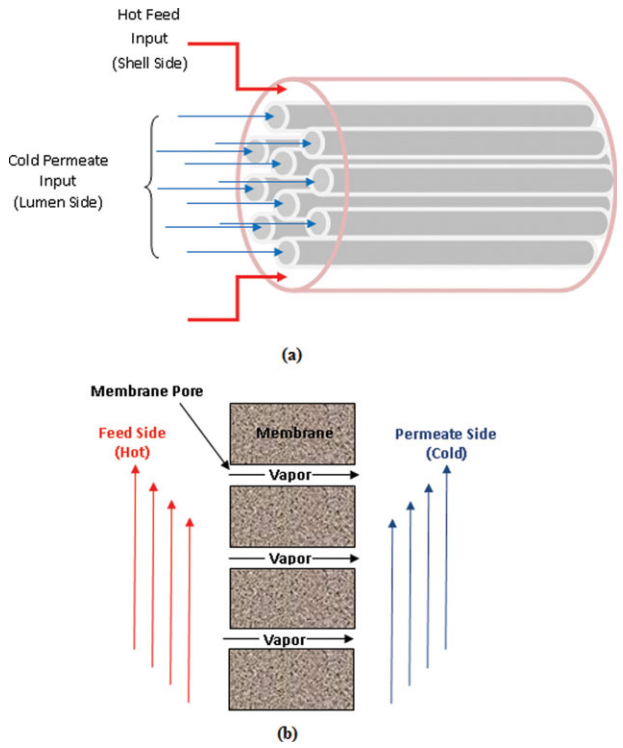

Figure 1. (a) DCMD hollow fiber membranes module; (b) DCMD.

[Color figure can be viewed in the online issue, which is available at wileyonlinelibrary.com.]

membrane mass transfer coefficients were in the range 6–30%. Recently, Bui et al.[20] proposed a semiempirical model demonstrated a linear relationship between heat and mass fluxes and their respective driving forces, such as conductive heat flux against temperature gradient and mass flux against water vapor pressure difference. This modeling focused on heat and mass transfer in the shell side (feed side) of the hollow fiber module. The modeling procedure was developed by adopting the analogy between heat and mass transfer.

Some studies determines the MD coefficient (MDC) in their modeling approach by fitting the calculated flux to the experimental results at different feed inlet temperatures.[1,23] This approach normally gives good predictions with author's experimental data. Mostly, there are no comparisons with the experimental data of other literature to evaluate the performance of these models based on wide range of experimental data.

In this study, new modeling of the process of DCMD for desalination is presented using numerical iterative technique for solving the set of nonlinear equations resulted from heat and mass balances that govern this process. The present approach is based on dividing the module length into similar cells. Therefore, the system of the nonlinear equations that describe the transport mechanisms in DCMD are solved numerically for each cell to get a new model for prediction of water flux, surface temperatures and composition, feed and permeate temperatures profiles via the required input of the feed and permeate temperatures, flow rate and feed composition as operating conditions. The validity of the model is evaluated by performing a comparison between the results of experiments presented in literature with the results predicted by the present model.

Theoretical Model

MD is a complicated physical process in which both heat and mass transfer are involved. It is a thermally driven process in which a microporous membrane acts as a physical support separating a warm solution from a cooler chamber, which contains either a liquid or a gas. As the process is nonisothermal, vapor molecules will migrate through the membrane pores from the high to the low vapor pressure side;[17,19] that is, from the warmer to the cooler side as shown in Figure 1.

Generally, the transport mechanism of MD can be summarized in: evaporation of water at the hot feed side of the membrane, penetration of water vapor through the membrane pores, and condensation of water vapor transported at the permeate side of the membrane.[19]

The vapor diffusion path is limited to the thickness of the membrane, thereby, reducing mass and heat transfer resistances. Condensation within the pores is avoided by selecting suitable material for the membrane and appropriate temperature differences across the membrane. Both heat and mass transfer are taking place simultaneously in DCMD, resulting in a complex heat transfer mechanism. As a result, the mass transfer rate, or the permeate flux, affects both the heat flux and the heat transfer coefficients in both feed and permeate sides.[17,19,24]

The driving force for water vapor permeation through the membrane pores is the temperature difference between the feed/membrane interface temperature (T_M^F) and the permeate/membrane interface temperature (T_M^P) as shown in Figure 2. Because of the heat losses in DCMD process, the membrane/interface temperatures are different from the bulk temperatures. This could be considered as one of the DCMD process drawbacks. This temperature difference leads to a decrease from the theoretical driving force, which is defined as the difference between the bulk feed temperature (T_M^F) and the bulk permeate temperature (T_M^P). This phenomenon is known as temperature polarization. The temperature polarization coefficient (TPC) is defined as the ratio between the actual and theoretical driving force;[25] then, the TPC is expressed mathematically as follows

$$\mathrm{TPC} = \frac{T_M^F - T_M^P}{T_B^F - T_B^P} \tag{1}$$

Qtaishat et al.[19] reported the TPC in the range of 0.88–0.92, and Lawson and Lloyd[26] reported close TPC values to

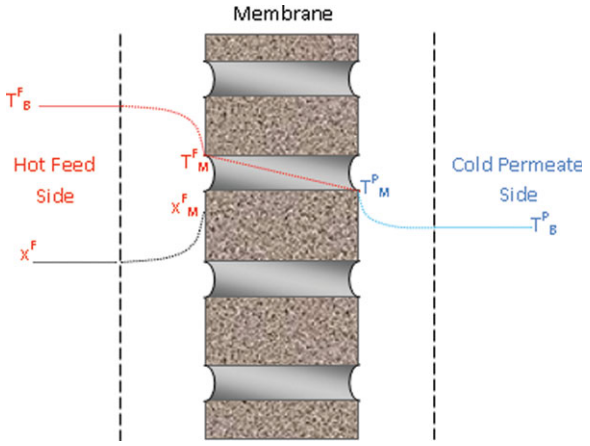

Figure 2. Heat and mass transfer in DCMD.

[Color figure can be viewed in the online issue, which is available at wileyonlinelibrary.com.]

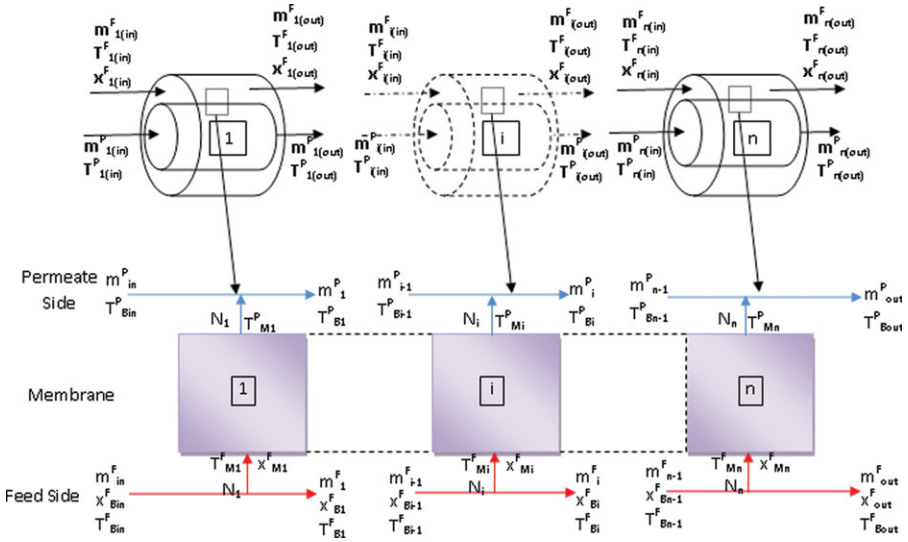

Figure 3. Schematic representations of the DCMD general concept cells.

[Color figure can be viewed in the online issue, which is available at wileyonlinelibrary.com.]

those achieved by Qtaishat et al.[19] This means that the temperature polarization effect is insignificant. The produced high values of TPC are due to the high values of the boundary layers' heat transfer coefficients, which reflect the high feed and permeate flow rates and the flow turbulence. Moreover, the values of TPC approach unity for well-designed systems as suggested by Lawson and Lloyd.[17,26]

Many assumptions are considered in the present model such as, there is no wetting occurs across the membrane, therefore, the rejection of the nonvolatile component in the feed is 100%. The vapor and liquid phases are in mechanical equilibrium (constant total pressure) and in thermodynamic equilibrium (corresponding to the temperature) at the interface at both feed and permeate side. The total pressure is constant along the water transport path of 1 atm, as a result of that the viscous (Poiseuille) flow mechanisms across the membrane is neglected. The entrapped air in the pores is static and the water vapor diffuses through it. The air is insoluble in water, due to low solubility of air in water.[19] A uniform pore size for whole membrane (pore size distribution was neglected). The water vapor is transported through a tortuous (not straight) cylinder.

The derivation of heat and mass transfer equations is based on dividing each single fiber in the module into (n) elements as shown in Figure 3, which illustrates the input and output of each element. As shown in Figure 2, the equations that govern the boundary layer heat and mass transfer are derived for the steady conditions. The amount of heat and mass transferred to and from the surface adjacent to the membrane are based on (as a typical configuration) the permeate stream in lumen side and the feed stream in shell side as shown in Figure 1a. The equations that govern the heat and mass transfer are listed below according to physical characteristics for each unit (cell i as a typical unit see Fig. 3) shell, lumen, and membrane side.

Shell Side (Feed as a Typical Stream)

Heat transfer

According to the basic principles of heat transfer, a thermal boundary layer will be formed when a fluid is brought into contact with a solid surface, if the temperatures of these two objects are different. The thermal boundary layer is adjacent to the solid surface, and it is assumed that only in this region does the fluid exhibit its temperature profile. This viewpoint is adopted to describe the MD process. Within the MD module, two fluids with different temperatures are separated by a microporous membrane (with the thickness of δ), therefore, two thermal boundary layers appear at the feed side and permeate side of the membrane, respectively, as shown in Figure 2.

According to Figure 3, the net of heat transferred in the boundary layer of the outer membrane surface is by convection and water vapor leaving the boundary layer. Thus

$$Q_i^{\mathrm{F}} = h_i^{\mathrm{F}} A_{\mathrm{ro}} (\overline{T}_{\mathrm{B}i}^{\mathrm{F}} - T_{\mathrm{M}i}^{\mathrm{F}}) - N_i A_{\mathrm{ro}} H_i^{\mathrm{FV}} \tag{2}$$

where i represents the cell number, N_i (kg/m^2 h) is the volatile component mass flux across the boundary layer of i cell based on outer surface area of the fiber. The boundary layer heat transfer coefficients are usually estimated from empirical correlations.[18,19] These correlations are shown in terms of dimensionless numbers: Nusselt, Reynolds, Prandtl, and heating/cooling correction factor as given in Table 1. Among these correlations the suitable heat transfer coefficient in the module shell side was estimated using Eq. 2a, which was correlated by Mengual et al.[31] for an external parallel flow along the fibers. This correlation was tested by the author for $400 < \mathrm{Re} < 2500$ with correlation coefficient of 0.996

$$\mathrm{Nu} = 0.042(\mathrm{Re})^{0.59}(\mathrm{Pr})^{0.33} \tag{2a}$$

$$\overline{T}_i^{\mathrm{F}} = \frac{T_{\mathrm{B}i}^{\mathrm{F}} + T_{\mathrm{B}i-1}^{\mathrm{F}}}{2} \tag{2b}$$

$$A_{\mathrm{ro}} = 2\pi r_{\mathrm{o}} l \tag{2c}$$

where, r_{o}, the outer radius of fiber, and l, the length of element = length of fiber/number of elements.

Based on the sensible enthalpy difference between the inlet and outlet of the main feed stream and the enthalpy of the water vapor transported to membrane side (see Fig. 3), energy balance in the feed side can be written as

$$Q_i^{\mathrm{F}} = m_{i-1}^{\mathrm{F}} H_{i-1}^{\mathrm{L}} - m_i^{\mathrm{F}} H_i^{\mathrm{L}} - N_i A_{\mathrm{ro}} H_i^{\mathrm{FV}} \tag{3}$$

Table 1. Correlations of Heat Transfer Coefficient that may be Useful in MD

Laminar Flow	Ref.	Turbulent flow	Ref.
$\mathrm{Nu} - 1.86\left(\frac{\mathrm{RsPr}}{L/D}\right)^{1/3}$	27	$\mathrm{Nu} = \left(1+\frac{6D}{L}\right)\left(\frac{(f/8)\mathrm{RePr}}{1.07+12.7(f/8)^{1/2}(\mathrm{Pr}^{2/3}-1)}\right)$	30
$\mathrm{Nu} = 4.36 + \left(\frac{0.0036\mathrm{RePr}(D/L)}{1+0.0011(\mathrm{RePr}(D/L))^{0.8}}\right)$	28	$\mathrm{Nu} = \left(1+\frac{6D}{L}\right)\left(\frac{(f/8)(\mathrm{Re}-1000)\mathrm{Pr}}{1+12.7(f/8)^{1/2}(\mathrm{Pr}^{2/3}-1)}\right)$	32
$\mathrm{Nu} = 0.13\mathrm{Re}^{0.645}\mathrm{Pr}^{0.38}$	29	$\mathrm{Nu} = 0.023\left(1+\frac{6D}{L}\right)\mathrm{Re}^{0.8}\mathrm{Pr}^{1/3}$	33
$\mathrm{Nu} = 1.95\left(\frac{\mathrm{RePr}}{L/D}\right)^{1/3}$	30	$\mathrm{Nu} = 0.036\mathrm{Re}^{0.8}\mathrm{Pr}^{1/3}\left(\frac{D}{L}\right)^{0.055}$	34
$\mathrm{Nu} = 0.097\mathrm{Re}^{0.73}\mathrm{Pr}^{0.13}$	29	$\mathrm{Nu} = \left(1+\frac{6D}{L}\right)\left(\frac{(f/8)\mathrm{RePr}}{1.2+13.2(f/8)^{1/2}(\mathrm{Pr}^{2/3}-1)}\right)$	35
$\mathrm{Nu} = \left(3.66 + \frac{0.0668\ G_z}{1+0.04(G_z)^{2/3}}\right)$	31	$\mathrm{Nu} = 0.027\left(1+\frac{6D}{L}\right)\mathrm{Re}^{0.8}\mathrm{Pr}^{1/3}\left(\frac{\mu}{\mu_w}\right)^{0.14}$	35
$\mathrm{Nu} = 3.66 + \left(\frac{0.104\mathrm{RePr}(D/L)}{1+0.0106(\mathrm{RePr}(D/L))^{0.8}}\right)$	30	$\mathrm{Nu} = 0.042(\mathrm{Re})^{0.59}(\mathrm{Pr})^{0.33}$,	31
$\mathrm{Nu} = 11.5(\mathrm{RePr})^{0.23}(D/L)^{0.5}$ for cooling $\mathrm{Nu} = 15(\mathrm{RePr})^{0.23}(D/L)^{0.5}$ for cooling	29	Note: $f = [0.79\ln(\mathrm{Re}) - 1.64]^{-2}$ for all correlations	

where, H, enthalpy of water liquid and vapor in kJ/kg, was estimated by Eqs. 3a and 3b given by Imdakm[36] T, temperature in K in the range of 273–373 K

$$H^L(T) = -1117.8 + 4.0312T + 2.0 \times 10^{-4}T^2 \quad (3a)$$

$$H^V(T) = 1850.7 + 2.8273T - 1.6 \times 10^{-3}T^2 \quad (3b)$$

Mass transfer

In fact, there are two steps to mass transfer in DCMD process: The volatile component passes through the concentration boundary layer (the region near the membrane surface, where the concentration profile of volatile and nonvolatile components is established) on the hot-side of the membrane and the second through the microporous membrane itself.

As shown in Figure 2, the composition of nonvolatile component increases from x^{F} to $x_{\mathrm{M}}^{\mathrm{F}}$ in the concentration boundary layer. Buildup of components in the concentration boundary layer due to the mass transfer resistance is referred to as concentration polarization. For a given bulk concentration, the presence of concentration boundary layer reduces the driving force for the volatile component to pass through the membrane, and thus, decreases the transmembrane mass flux.

The mass flux of species (volatile component) through the concentration boundary layer of nonvolatile component (Fig. 2) may be calculated according to the theory of mass transfer in boundary layer from the following equation[17]

$$N_i = -k_i^{\mathrm{F}} C_{\mathrm{T}} \mathrm{Mwt_w} \ln\left(\frac{x_{\mathrm{M}i}^{\mathrm{F}}}{\overline{x}_{\mathrm{B}i}^{\mathrm{F}}}\right) \quad (4)$$

$$\overline{x}_{\mathrm{B}i}^{\mathrm{F}} = \frac{x_{\mathrm{B}i}^{\mathrm{F}} + x_{\mathrm{B}i-1}^{\mathrm{F}}}{2} \quad (4a)$$

where N_i (kg/m^2 h) mass flux of volatile component, C_{T} (kmol/m^3) is the total concentration at the feed bulk, and x^{F} is the mole fraction of nonvolatile component at feed side, and k_i^{F} (m/h) is the mass transfer coefficient usually estimated from the analogy between heat and mass transfer using the correlations given in Table 1 by substituting the Sherwood number ($k{\cdot}D/D_{\mathrm{AB}}$) for the Nusselt number, Schmidt number ($\mu/\rho{\cdot}D_{\mathrm{AB}}$) for the Prandtl. This assumption is generally accepted due to the similarity of the two transport processes occurring in the same geometry.[20]

As long as no wetting occurs, the membrane used in MD can 100% rejects the nonvolatile component; therefore, a component mass balance on the nonvolatile component in the feed side yields Eq. 5 (Fig. 3)

$$\text{Component material balance}: \frac{m_i^{\mathrm{F}}}{(\mathrm{Mwt_{sol}})_i} x_i^{\mathrm{F}} = \frac{m_{i-1}^{\mathrm{F}}}{(\mathrm{Mwt_{sol}})_{i-1}} x_{i-1}^{\mathrm{F}}$$

Thus

$$x_i^{\mathrm{F}} = \frac{m_{i-1}^{\mathrm{F}}}{m_i^{\mathrm{F}}} \frac{(\mathrm{Mwt_{sol}})_i}{(\mathrm{Mwt_{sol}})_{i-1}} x_{i-1}^{\mathrm{F}} \quad (5)$$

Total mass balance in the feed side (Fig. 3)

$$m_{i-1}^{\mathrm{F}} = m_i^{\mathrm{F}} + N_i A_{\mathrm{ro}} \quad (6)$$

Lumen Side (Permeate as a Typical Stream)

Heat transfer

In thermal boundary layer in the permeate side (inner surface), the heat is transferred by convection and mass transfer contribution (Fig. 3). Thus

$$Q_i^{\mathrm{P}} = h_i^{\mathrm{P}} A_{ri} (T_{\mathrm{M}i}^{\mathrm{P}} - \overline{T}_{\mathrm{B}i}^{\mathrm{P}}) + N_i A_{\mathrm{ro}} H_i^{\mathrm{PV}} \quad (7)$$

On the lumen side, heat transfer model for laminar flow (Re $<$ 2100) within a cylindrical pipe expressed using (Sieder–Tate model) Eq. 7a and Hausen model Eq. 7b[37–39] as mentioned in Bui et al.[20]

$$\mathrm{Nu} = 1.86\left(\frac{\mathrm{Re\,Pr}}{L/D}\right)^{1/3}\left(\frac{\mu}{\mu_{\mathrm{W}}}\right)^{0.14} \text{ if } \mathrm{Gz} = 100 \quad (7a)$$

$$\mathrm{Nu} = \left(3.66 + \frac{0.0668 G_{\mathrm{z}}}{1 + 0.04(G_{\mathrm{z}})^{2/3}}\right)^{1/3}\left(\frac{\mu}{\mu_{\mathrm{W}}}\right)^{0.14} \text{ if } \mathrm{Gz}<100 \quad (7b)$$

$$G_{\mathrm{z}} = \mathrm{Re\ Pr}\,\frac{D}{L} \quad (7c)$$

The energy balance in the permeate side is due to the sensible heat difference between the inlet and outlet of the main permeate stream and the enthalpy of the water vapor transported from membrane side. Thus

$$Q_i^{\mathrm{P}} = m_{i-1}^{\mathrm{P}} H_{i-1}^{\mathrm{L}} - m_i^{\mathrm{P}} H_i^{\mathrm{L}} + N_i A_{\mathrm{ro}} H_i^{\mathrm{PV}} \tag{8}$$

Mass transfer

Because 100% of the nonvolatile components are rejected by the membrane, therefore, it can be assumed that there is no concentration boundary layer formed at the permeate side of the membrane.

Total mass balance in the permeate side (Figure 3)

$$m_{i-1}^{\mathrm{P}} = m_i^{\mathrm{P}} - N_i A_{\mathrm{ro}} \tag{9}$$

Membrane side

Heat transfer

The heat inside the membrane is transferred by conduction across the membrane material (heat losses) and together with a vapor flowing through the membrane.

The heat transfer in the membrane side is by conduction (in solid and fluid) and water vapor transports across the membrane through the pores. Thus

$$Q_i^{\mathrm{M}} = h_i^{\mathrm{M}} A_{r\,\ln}\left(T_{\mathrm{M}i}^{\mathrm{F}} - T_{\mathrm{M}i}^{\mathrm{P}}\right) + N_i A_{\mathrm{ro}}\left(H_i^{\mathrm{FV}} - H_i^{\mathrm{PV}}\right) \tag{10}$$

$$A_{\mathrm{r\,ln}} = (A_{\mathrm{ro}} - A_{ri}) / \ln\left(\frac{A_{\mathrm{ro}}}{A_{ri}}\right) \tag{10a}$$

where, h^{M} is the heat transfer coefficient of the hydrophobic membrane, which can be calculated from the thermal conductivities of the hydrophobic membrane polymer (k^{M}) and water vapor and air trapped inside the membrane pores (k^{G}). There are three models that can be used to predict the thermal conductivity of two-phase composite material, based on molecular orientation: (1) the Isostrain or parallel model; (2) Isostress or series model; (3) flux law model[22]

$$h^{\mathrm{M}} = \frac{k^{\mathrm{G}}\varepsilon + k^{\mathrm{M}}(1-\varepsilon)}{\delta} \quad \text{Isostrain or parallel model} \tag{10b1}$$

$$h^{\mathrm{M}} = \frac{\left[\frac{\varepsilon}{k^{\mathrm{G}}} + \frac{(1-\varepsilon)}{k^{\mathrm{M}}}\right]^{-1}}{\delta} \quad \text{Isostress or parallel model} \tag{10b2}$$

$$h^{\mathrm{M}} = \frac{k^{\mathrm{G}}}{\delta}\left[\frac{1 + (1-\varepsilon)\left(\frac{k^{\mathrm{M}}}{k^{\mathrm{G}}} - 1\right) / \left(\frac{k^{\mathrm{M}}}{k^{\mathrm{G}}} + 2\right)}{1 - (1-\varepsilon)\left(\frac{k^{\mathrm{M}}}{k^{\mathrm{G}}} - 1\right) / \left(\frac{k^{\mathrm{M}}}{k^{\mathrm{G}}} + 2\right)}\right] \quad \text{Flux law model} \tag{10b3}$$

where δ and ε are the thickness and porosity of the hydrophobic membrane, respectively.

Phattaranawik et al.[22] used different types of membrane with different pore size and showed that the Isostress or parallel model Eq. 10b2 appeared to be the most appropriate model for calculating the membrane thermal conductivity and the same result has been achieved in our simulation. Eqs. 10c and 10d were given by Lawson and Lloyd[17], and Eqs 10e–10g were correlated using curve fitting, for membrane polymer where T is in K in the operation range of DCMD. These equations are valid at temperature range 273–373 K

$$k_{\mathrm{water}}^{\mathrm{G}}(T) = 2.72 \times 10^{-3} + 5.71 \times 10^{-5} T \tag{10c}$$

$$k_{\mathrm{air}}^{\mathrm{G}}(T) = 2.72 \times 10^{-3} + 7.77 \times 10^{-5} T \tag{10d}$$

$$k_{\mathrm{PVDF}}^{\mathrm{M}}(T) = 9.2308 \times 10^{-3} + 5.77 \times 10^{-4} T \tag{10e}$$

$$k_{\mathrm{PTFE}}^{\mathrm{M}}(T) = 0.087 + 6 \times 10^{-4} T \tag{10f}$$

$$k_{\mathrm{PP}}^{\mathrm{M}}(T) = -0.248 \times 10^{-3} + 1.3 \times 10^{-3} T \tag{10g}$$

At steady state

$$Q^{\mathrm{F}} = Q^{\mathrm{M}} = Q^{\mathrm{P}} \tag{11}$$

The equations for the determination of the temperatures of the surface adjacent to the membrane $T_{\mathrm{M}i}^{\mathrm{F}}$ and $T_{\mathrm{M}i}^{\mathrm{P}}$ presented so far in the literature were derived with the assumption of the linear temperature change in the membrane and isenthalpic flow of vapor. With such assumption, the equations describing the heat stream density flowing across the membrane combining with boundary layer equations leads to

$$T_{\mathrm{M}i}^{\mathrm{F}} = \frac{h^{\mathrm{M}}[T_i^{\mathrm{P}} + (h^{\mathrm{F}}/h^{\mathrm{P}})T_i^{\mathrm{F}}] + h^{\mathrm{F}} T_i^{\mathrm{F}} - N_i H_i^{\mathrm{V}}}{h^{\mathrm{M}} + h^{\mathrm{F}}[1 + (h^{\mathrm{M}}/h^{\mathrm{P}})]} \tag{12}$$

$$T_{\mathrm{M}i}^{\mathrm{P}} = \frac{h^{\mathrm{M}}[T_i^{\mathrm{F}} + (h^{\mathrm{P}}/h^{\mathrm{F}})T_i^{\mathrm{P}}] + h^{\mathrm{P}} T_i^{\mathrm{P}} + N_i H_i^{\mathrm{V}}}{h^{\mathrm{M}} + h^{\mathrm{P}}[1 + (h^{\mathrm{M}}/h^{\mathrm{F}})]} \tag{13}$$

Mass transfer

The mass transfer in the DCMD process is usually described by assuming a linear relationship between the mass flux (N) and the water vapor pressure difference through the MDC (K_i^{M}). Thus

$$N_i = K_i^{\mathrm{M}}\left(p_{\mathrm{M}i}^{\mathrm{F}} - p_{\mathrm{M}i}^{\mathrm{P}}\right) \tag{14}$$

where $p_{\mathrm{M}i}^{\mathrm{F}}$ and $p_{\mathrm{M}i}^{\mathrm{P}}$ are the partial pressures of water at the feed and permeate sides evaluated, according to the assumption of thermodynamic equilibrium at the interface at both feed and permeate side by Lawson and Lloyd[17] and Teoh et al.[40]

$$p_{\mathrm{M}i}^{\mathrm{F}} = \left(1 - x_{\mathrm{M}i}^{\mathrm{F}}\right)\alpha_i P^{\mathrm{VF}} \tag{14a}$$

$$p_{\mathrm{M}i}^{\mathrm{P}} = P^{\mathrm{VP}} \tag{14b}$$

α is the water activity coefficient in an aqueous sodium chloride solution estimated by Lawson and Lloyd.[17]

$$\alpha_i = 1 - 0.5 x_{\mathrm{M}i}^{\mathrm{F}} - 10\left(x_{\mathrm{M}i}^{\mathrm{F}}\right)^2 \tag{14c}$$

P^{V} is the water vapor pressure estimated by Antoine equation at the temperatures $T_{\mathrm{M}i}^{\mathrm{F}}$ and $T_{\mathrm{M}i}^{\mathrm{P}}$, for feed and permeate respectively, as follow

$$P^{\mathrm{V}} = \exp\left(23.328 - \frac{3841}{T - 45}\right) \tag{14d}$$

where P^{V} in Pascal and T is the corresponding temperature in K.[41] This equation is valid at temperature range 273–373 K.[19]

Various types of mechanisms have been proposed for the transport of gases or vapors through porous membranes: the Knudsen model, viscous model, ordinary-diffusion model, and/or a combination of them. Because of the fact that in DCMD process both the hot feed and cold permeate water are brought into contact with the membrane under atmospheric pressure, the total pressure is constant at about 1 atm, resulting in a negligible viscous flow.[42,43]

The Knudsen number, Kn, is the governing quantity that provides a guideline in determining which mechanism is operative under a given experimental condition and defined as the ratio of the mean free path (λ) of the transported molecules to the pore size (diameter, d) of the membrane, that is, Kn = λ/d.

It has been assumed that the entrapped air in the pores is static and the water vapor diffuses through it. The air is insoluble in water, due to low solubility of air in water.[19] Therefore, for the binary mixture of water vapor and air, the mean molecular free path of water in air (λ_{W-A}) is evaluated at the average surface membrane temperature at feed and permeate side ($\overline{T}_{Mi}^{F-P}$)[44]

$$\lambda_{W-A} = \frac{k_B \overline{T}_{Mi}^{F-P}}{\pi\left(\frac{\sigma_W+\sigma_A}{2}\right)^2 P_T \sqrt{1+\left(\frac{Mwt_W}{Mwt_A}\right)}} \tag{15}$$

where k_B is the Boltzmann constant (1.381×10^{-23} J K^{-1}), P_T is the total absolute pressure (Pa), σ_W and σ_A are the collision diameters for water vapor (2.641×10^{-10} m) and air (3.711×10^{-10} m),[45] and Mwt_W and Mwt_A are the molecular weights of water and air respectively. At the typical membrane temperature of 60°C and pressure of 1.013×10^5 Pa in DCMD, the mean free path of water in air is 0.182 μm larger than the pore diameter (based on outer surface) on the membrane surface for most hollow fibers used for DCMD. Therefore, the combination of Knudsen diffusion and molecular diffusion of vapor transfer through the membrane pores is almost responsible for mass transfer in DCMD.[42,46]

In DCMD, mass transfer across the membrane occurs in three regions depending on the pore size and the mean free path of the transferring species[42]: Knudsen region, continuum region (or ordinary-diffusion region) and transition region (or combined Knudsen-/ordinary-diffusion region). If the mean free path of transporting water molecules is large in relation with the membrane pore size (i.e., Kn $>$ 1 or $d < \lambda$), the molecule–pore wall collisions are dominant over the molecule–molecule collisions and a Knudsen type of flow will be the prevailing mechanism that describes the water vapor migration through the membrane pores.

In the DCMD process, air is always entrapped within the membrane pores with pressure values close to the atmospheric pressure. Therefore, if Kn $<$ 0.01 (i.e., $d > 100\ \lambda$), molecular diffusion is used to describe the mass transfer in continuum region caused by the virtually stagnant air trapped within each membrane pore due to the low solubility of air in water.

Finally, in the transition region, 0.01 $<$ Kn $<$1 molecules of water collide with each other and diffuse among the air molecules. In this case, the mass transfer takes place via the combined Knudsen-/ordinary-diffusion mechanism, and the following equation is used to determine the water liquid permeability. In any of these cases, with assuming the uniform pore size for the whole membrane, the net DCMD membrane permeability can be expressed as follows[42,43]

$$K_i^M = \begin{cases} \beta_i^K & \text{kn}<0.01 \\ \beta_i^{MD} & \text{kn} > 1.00 \\ \beta_i^{K-MD} & 0.01<\text{kn}<1.00 \end{cases} \tag{16}$$

$$\beta_i^K = \frac{2r}{3}\frac{\varepsilon}{\tau\delta}\frac{Mwt_W}{RT}\left(\frac{8RT}{Mwt_W}\right)^{1/2} \tag{16a}$$

$$\beta_i^{MD} = \frac{\varepsilon}{\tau\delta}\frac{Mwt_W}{RT}\left(\frac{PD_{WA}}{(p_a)_{lm}}\right) \tag{16b}$$

$$\beta_i^{K-MD} = \left[\frac{1}{\beta_i^K}+\frac{1}{\beta_i^{MD}}\right]^{-1} \tag{16c}$$

where ϵ, τ, r, and δ are the porosity, pore tortuosity, pore radius and thickness of the hydrophobic membrane, respectively; R is the gas constant and T is the absolute temperature, Pa is the air pressure, P is the total pressure inside the pore assumed constant and equal to the sum of the partial pressures of air and water liquid, and D_{WA} is the water diffusion coefficient in air. The value of PD_{WA} (Pa m^2/s) for water–air is calculated using the following expression, which is valid in temperature range 273–373 K.[42,43]

$$PD_{WA} = 1.895\ 10^{-5} T^{2.072} \tag{16d}$$

Mathematical Model

To build up a suitable mathematical model for the MD, it is very important to have a good knowledge about the heat and mass transfer mechanisms in this process. Mathematical model of MD is necessary for understanding the process and acting as an infrastructure for industrial design. It focuses on the description of the heat and mass transfers. In what follows, how to deduce the model equations and analyze the MD performance according to the solution of these equations are clarified. The primary purpose of the model is to predict the values of the permeate flux and its dependence on the membrane module design, membrane parameters and operating variables.[47]

A number of unknown variables should be firmly determined to improve our analysis and understanding of DCMD process; these unknowns are mainly the average permeate flux along the module, the outlet temperatures of feed and permeate streams, and the outlet concentration of the feed stream. These results are based on the calculation of heat transfer coefficients of the boundary layers (h^F and h^P), Membrane–liquid interface temperatures (T_M^F and T_M^P), membrane conductive heat transfer coefficient (h^M) and MDC (K^M). Generally, in the literature the evaluation of these unknowns depend on the empirical evaluation of the heat transfer coefficients of the boundary layer, which is followed by the evaluation of the membrane interface temperatures using a simple heat balance. The evaluation of the heat transfer coefficient of the membrane depends on the membrane characterizations such as; porosity, thickness, the thermal conductivities of the membrane polymer and entrapped gas as shown in Eq. 10b. The MDC could be estimated using the membrane properties, that is, mean pore size, porosity, tortuosity, etc. according to Eq. 16.

The set of nonlinear equations resulted from heat and mass balances on each cell of a train of a multicells shown in Figure 3, is solved using a numerical solution. As it can be seen, the measured and estimated parameters of the cell 1

Table 2. Specifications and Operating Conditions of the Hollow Fiber Modules Used in DCMD Experiments

Membrane Type	Polypropylene	PVDF	PVDF	Pure PVDF	PVDF T30	PVDF T50	PVDF T50A	PVDF T50B	PVDF T50C
ID (mm)	1.8	0.52	0.6	0.68	0.692	0.69	0.63	0.585	0.53
OD (mm)	2.6	1.2	0.82	0.96	0.982	0.98	0.91	0.845	0.75
Shell diam. (cm)	2	0.95	0.95		0.95			0.95	
Length (cm)	20	17	20		17			17	
Pore size (μm)	0.2	0. 41	0.16	0.161	0.136	0.116	0.186	0.191	0.248
Porosity	0.73	0.8	0.8	0.86	0.81	0.74	0.73	0.76	0.8
No. of fibers	15	10	65	40	40				
Inlet feed temperature (°C)	85	50–90	30–80		50–80			50–80	
Inlet permeate temperature (°C)	20	16.5	17.5		17.5			17.5	
Salt Concentration (wt %)	1.6	3.5	3.5		3.5			3.5	
Feed flow rate	14 cm^3/s	33.5 cm^3/s	1.6 m/s		1.94 m/s			1.94 m/s	
Permeate flow rate	14 cm^3/s	1.7 cm^3/s	0.8 m/s		0.95 m/s			0.95 m/s	
Liquid in lumen side	Feed	Feed	Permeate		Permeate			Permeate	
Permeate flux data	6	5	5	4	4	4	4	4	4
Temperature data		5	10						
Reference	51	48	6				40		

	PVDF			PVDF/clay			Polypropylene	
Membrane Type	Kur_A	Kur_B	Kur_C	Kur_A	Kur_B	Kur_C	M1	M2
ID (mm)	0.76	0.92	1.02	0.8	0.96	1.02	1.8	
OD (mm)	1.2	1.29	1.34	1.3	1.36	1.38	2.61	
Shell diam. (cm)		0.95			0.95		0.7	
Length (cm)		20			20		59	
Pore size (μm)		0.6			0.6		0.1252	0.1077
Porosity	0.917	0.901	0.896	0.889	0.876	0.867	0.734	0.748
No. of fibers		20			20		3	
Inlet feed temperature (°C)		40–80			40–80		40–81	60–85
Inlet permeate temperature (°C)		17.5			17.5		20	
Salt concentration (wt %)		3.5		3.5		0–14	Tap water	
Feed flow rate		1.8 m/s		1.8 m/s		0.4–1.8 m/s	0.42 m/s	0.96–0.42 m/s
Permeate flow rate		1.2 m/s		1.2 m/s		0.3–1.3 m/s	0.29 m/s	
Liquid in lumen side		Permeate			Permeate		Feed	
Permeate flux data	5	5	5	5	5	20	4	8
Reference			46				49	

are the inlet temperature and mass flow rate of the feed and permeate side stream, and the inlet salt concentration of the feed side stream. These parameters are used as input data to the developed program written by MATLAB® code to solve the set of nonlinear simultaneous equations. The outputs of the developed program for each cell are; at the feed side: outlet temperature, mass flow rate, the membrane surface temperature and salt concentration, whereas, at the permeate side: outlet temperature, mass flow rate, and the membrane surface temperature as well as the permeation flux and the rate of heat transferred across the membrane. A system of 10 nonlinear equations has been solved simultaneously to predict the ten-stated unknown's variables using the FSOLVE coding, which is a built-in function in MATLAB®. This coding uses the least square method as a numerical technique for solving a system of nonlinear equations. These equations were 2–10 and 14.

The elapsed time for solution is greatly depending upon the number of cells assumed. The number of cells ($n = 10$) was suitable for all experimental data. The elapsed time was between 10 and 15 s for temperatures less than 85°C and between 25 and 35 s for more than 85°C when the number of cells was $n = 10$ for each predicted point.

Results and Model Validation

The prediction results of the present model were compared with various experimental data of various membrane specifications, types, operating conditions. These experimental data were extracted from the literature and summarized in Table 2, to confirm that the model simulates the operation of DCMD, and 122 experimental data points of permeate fluxes and temperatures are used in this study for this purpose.

Effect of feed temperature

Most of the experimental data in the literature describe the effect of feed temperatures on the permeate flux. It is well known that the temperature in MD processes is the significant operating variable that affects the MD performance due to exponential increase of vapor pressure with temperature.[19]

Figure 4 shows a comparison of the effect of feed temperature on permeate flux of the experimental data of Bonyadi et al.[48] with the results calculated by the present model. These experimental data were obtained from the fabrication of dual layer hydrophilic–hydrophobic hollow fibers especially for DCMD process. The thickness of hollow fiber wall used in Bonyadi's study was composed of two layers; the hydrophilic layer with thickness of 330 μm and the hydrophobic layer of 50-μm thickness. The feed temperature range was between 50 and 90°C, and other characteristics parameters are shown in Table 2. It can be noticed that the permeate flux predicted by the present model is in a good agreement with the experimental data reported by Bonyadi et al.[48] and the average deviation between them is about 18%.

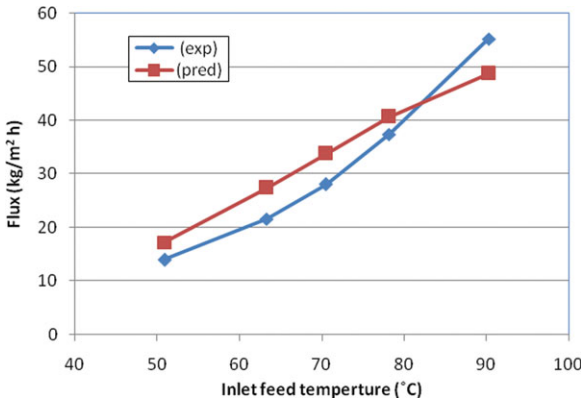

Figure 4. Effect of inlet feed temperature on permeate flux (τ = 1.8).[48]

[Color figure can be viewed in the online issue, which is available at wileyonlinelibrary.com.]

The main cause for the deviation between prediction and experiment results is due to the thickness of the additional hydrophilic layer, which is added another resistance to the mass transfer. The hydrophobic layer introduces an additional heat transfer resistance that amplifies the temperature polarization phenomenon, which is in return results in a decrease of temperature of the evaporation surface and as a consequence, the driving force of mass transfer and the permeate flux is reduced. That may explain the overestimation of the most simulation results. The underestimation of the last point is due to the effect of the tortuosity value, which leads to the linear trend of the simulated results compared with exponential trend of the experimental data of permeate flux against inlet feed temperature. The effect of tortuosity values will be demonstrated later.

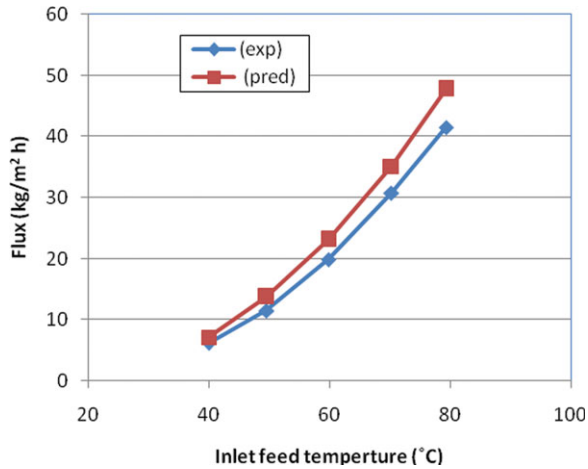

Figure 6. Effect of inlet feed temperature on permeate flux (τ = 3).[6]

[Color figure can be viewed in the online issue, which is available at wileyonlinelibrary.com.]

Comparison of the experimental data reported by Gryta[49] of the effect of feed temperature on permeate flux as a function of two different feed velocities, 0.96 and 0.42 m/s with the results predicted by the present model are shown in Figure 5. These experimental data are taken from two kinds of polypropylene capillary membranes (M1, and M2) used in the production of demineralized water from tap water. The membrane porosity of type M1 is about 73.4%, whereas the type M2 module is made from the membranes, which have an additional top layer, not to exceed 1 μm, with membrane porosity 74.8%. The temperature of the feed solution is between 60 and 85°C. It can be noticed that the permeate flux decreased with the decreasing of the feed velocity from

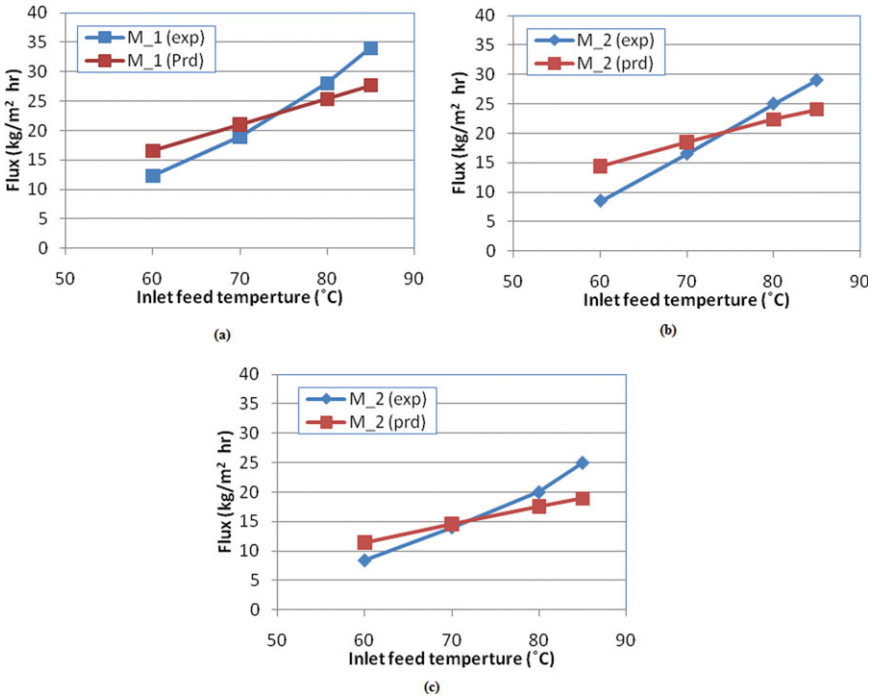

Figure 5. Effect of inlet feed temperature on permeate flux (τ = 1).[49]

(a), (b) feed velocity 0.96 m/s, and (c) feed velocity 0.42 m/s. [Color figure can be viewed in the online issue, which is available at wileyonlinelibrary.com.]

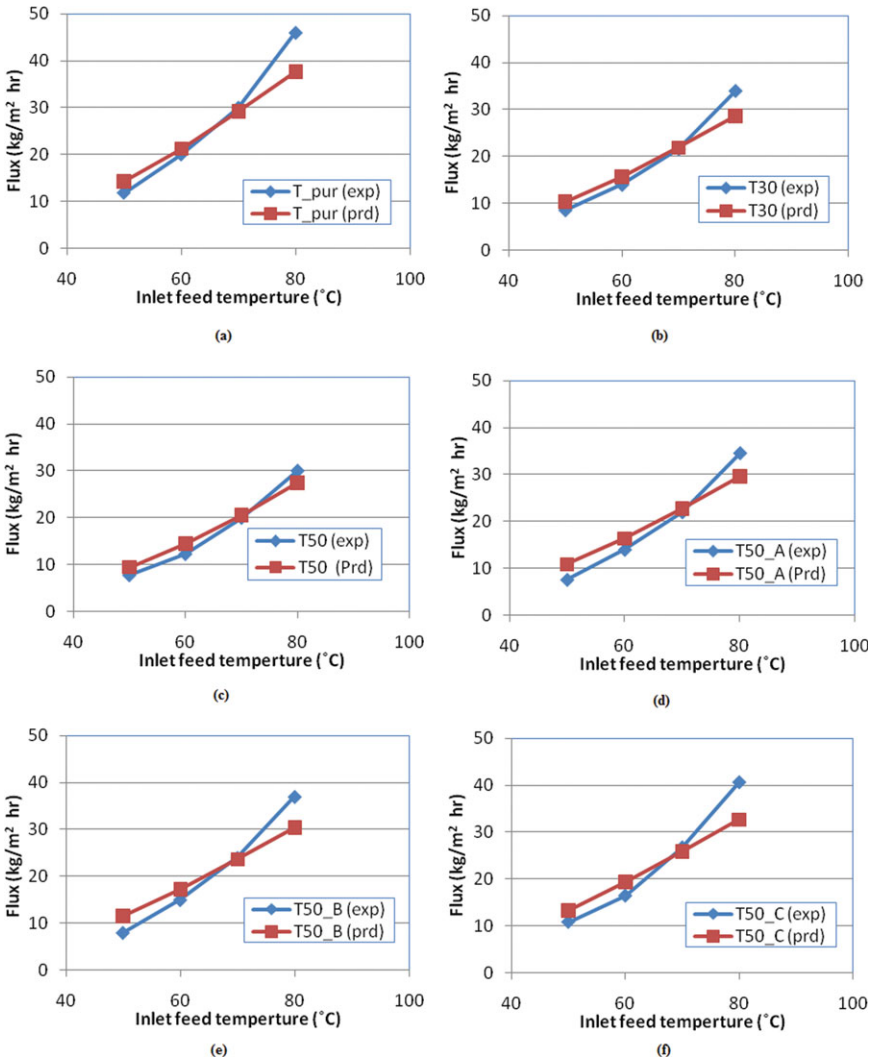

Figure 7. Effect of inlet feed temperature on permeate flux (τ = 3 for a, = 2.5 for other)[40] (a) pure PVDF, (b) 30 wt % PTFE additive, (c) 50 wt % PTFE additive, (d) 50 wt % PTFE additive using 0.5-cm air gap, (e) 50 wt % PTFE additive using 2-cm air gap, and (f) 50 wt % PTFE additive using 4-cm air gap.

[Color figure can be viewed in the online issue, which is available at wileyonlinelibrary.com.]

0.96 to 0.42 m/s for type M2 as shown in Figures 5b, c, respectively. The average deviation between the permeation fluxes predicted by the present model and these experimental data for membrane is 17% for type M1. Whereas the deviation between them using membrane type M2 is 27% when using 0.96 m/s as a feed velocity, and 19% when using o.42 m/s. From these results, it can be concluded that the results calculated by the present model are in a fair agreement with the experimental data reported by Gryta.[49] The wide pore size distribution of M1 and M2 is the main reason for the deviation between the predicted permeates flux of the present model and experimental data. The presence of additional polymeric thin layer with low surface porosity on the internal surface (feed side) of the membrane (M2) decline the permeate flux. The author stated that the SEM examinations of cross-sections of the membranes taken for autopsy from M1 module revealed that the $CaCO_3$ deposit covered not only the membrane surfaces but also was deposited into the pores, while in the case of the membranes having a low surface porosity (M2) the $CaCO_3$ deposit was formed mainly on the membrane surface. That may demonstrate the overestimation of the permeate flux at lower inlet feed temperature. The underestimation at higher inlet feed temperature is due to the linear trend of the simulated results due to the effect of the tortuosity value.

Figure 6 shows the influence of feed temperature on permeates flux found by Wang et al.[6] and by the present model. Poly(vinylidene flouride) (PVDF) hollow fiber membranes prepared using ethylene glycol (EG) as additive had an ultrathin skin layer and a porous support layer. The addition of EG as additive was to improve the PVDF membrane porosity with narrow mean pore size induced, and to enhance pore formation during phase inversion process thereby enhancing the performance of the membrane. From Figure 6, it can be noticed that the predicted results from the present model were in a good agreement with the experimental results reported by Wang et al.[6] and the average deviation between them is about 16%. The PVDF hollow fiber has an ultrathin skin layer (less than 10 nm) with small surface porosity. The presence of this ultra skin layer is the main reason for limiting the permeate flux of the membrane and this maybe the reason for the overestimation of the simulation results.

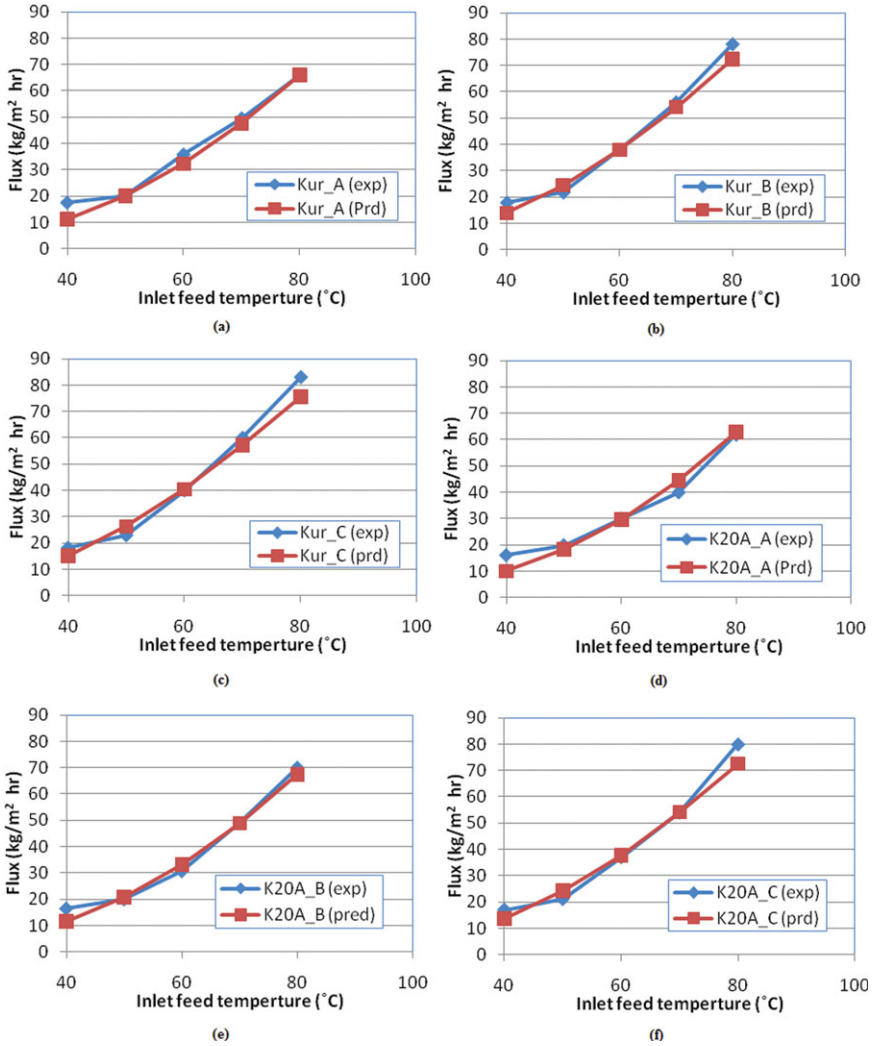

Figure 8. Effect of inlet feed temperature on permeate flux (τ = 3 for a, d, e and = 2.5 for other).[46]

The membrane materials was Kureha PDVF1300 resin a, b, c PVDF/NMP/EG (10/78/12) wt % were varied in membrane thickness. d, e, f PVDF/NMP/Cloisite 20A/EG (10/74.7/3.3/12) wt %. [Color figure can be viewed in the online issue, which is available at wileyonlinelibrary.com.]

The comparison between the results predicted by the model and experimental results found by Teoh et al.[40] regarding the effect of feed temperature on the permeate flux is shown in Figure 7. These experimental data have been summarized from many types of hollow fiber membranes prepared for desalination via DCMD. The hollow fiber membranes prepared from pure PVDF, are 30 wt % (T30) and 50 wt % (T50) particle loading of PTFE, and the latter prepared using different air gap distance, such as, 0.5 cm (T50_A), 2 cm (T50_B), and 4 cm (T50_C). The specifications of the fibers are shown in Table 2. From Figure 7a, it can be noticed that the pure PVDF hollow fiber shows higher permeation flux than the other hollow fibers shown in Figure 7b–f at the same operating conditions. The hollow fiber membrane prepared from 30 wt % PTFE (T30) exhibited higher permeation flux than that prepared from 50 wt % PTFE (T50) and the others are in the order: (T50_A) > (T50_B) > (T50_C). The reason for the differences in permeation fluxes for all membrane types is due to the variation of characteristics of membrane such as porosity and mean pore size of the membrane (see Eq. 17). Figure 7 shows that the experimental results are in a good agreement with that predicted by the present model. The average deviations between the theoretical and experimental results are as follows: 11, 12, 12, 19, 19, and 15%, for pure PVDF, (T30), (T50), (T50_A), (T50_B), and (T50_C), respectively. The values of membrane characterizations such as pore size distribution, mean pore diameters, membrane wall thickness and surface porosity play very important role in the calculation of the permeation flux as demonstrated later. In fact these values of characterizations were supplied by the manufacturer and there is a level of uncertainty.[19] This reason may explain the deviations between the simulation and experiment results.

Figure 8 shows the comparison of the model results with experimental data reported by Wang et al.[46] These experimental data have been collected from two types of hollow fiber membranes fabricated from PVDF/EG (Kur_A, Kur_B, and Kur_C) and PVDF/EG/Cloisite clay composite (K20A_A, K20A_B, and K20A_C) which have porosity up to 90% and the other membrane characteristics are given in Table 2. Addition of EG as a pore-forming agent in dope solution is to form a thin skin layer and produce membranes with a porous structure. The other additive is clay particles as they can reinforce fiber mechanical strength and control the coefficients of thermal expansion and heat insulation by

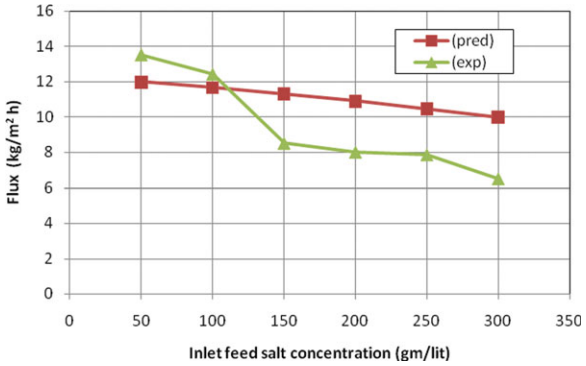

Figure 9. Effect of inlet salt concentration on permeate flux ($\tau = 3$).[51]

[Color figure can be viewed in the online issue, which is available at wileyonlinelibrary.com.]

forming a kind of mixed matrix membrane embedded with a dispersed inorganic phase.[50] The feed temperature was in the range between 40 and 80°C. Figure 8 shows a good agreement between the data of experiments and that of the present model. The average deviations are as follows: 10% for Kur_A, 9% for Kur_B, 9% for Kur_C, 12% for K20A_A, 9% for K20A_B, and 9% for K20A_C. The percentage error between the predicted results by the model and experimental results may be due to the membrane structure. The membrane consists of three layers, where a thin layer full of sponge-like structure is located between two thick layers full of finger-like macrovoids, this will affect the membrane tortuosity which in turn affect the membrane performance.

Effect of salt concentration

Some researchers reported the effect of salt concentration on the permeation flux of the hollow fiber membranes.[19,46,51] In this study, the estimated results by the present model have been compared with the experimental results reported by the researchers.[46,51] Figure 9 shows the effect of salt concentration in the feed solution on the permeation flux. From this Figure, it can be seen that the water permeation flux decreases with increasing salt concentration in feed solution within the concentration range 50–300 g/l as reported by Gryta et al.[51] The feed solution temperatures were 85 and 20°C for the permeate side, and the feed flow rate was 14 cm^3/s. The decline in permeation flux of the experimental results at high salt concentrations is due to the deposition of organic matter on the membrane surface as was observed by the authors. For this reason, the deviation between the predicted results and that reported by the authors was about 29%. The change in the permeation flux is about 52% for the experimental data as a function of salt concentration changed from 50 to 300 gm/l, whereas it is 16% for the presented model as shown in Figure 9. Our predicted result agrees with that reported by Qtaishat et al.[19] They found that the water permeation flux through the membrane affected slightly by the change of initial salt concentration, the permeation flux decreased by about 12% when the NaCl concentration in feed solution was increased from 0 to 2 M.

Figure 10 demonstrates the Wang et al.[46] experimental results and theoretical results by presented model of the permeate flux as a function of the concentration of NaCl (wt %) in feed solutions under 60°C, 1.8 m/s, and 17.5°C inlet temperature and 1.2 m/s for permeate stream. As reported by Wang et al.,[46] there is a 21.5% decrease in flux when 14 wt % NaCl concentration in feed solution (four times higher than sea water concentration). The reduction of water vapor pressure under high solute concentrations is the main reason for the decrease in permeation flux under the same temperature. The comparison between the experimental data reported by Wang et al.[46] and the predicted results by the new model is found to be in a good agreement with 6% average deviation as shown in Figure 10. There is an overprediction of the simulation results as shown in Figure 10. This is attributed to the increase of NaCl concentration on the membrane surface that decrease the membrane surface temperature due to concentration and thermal polarization, which in turn reduced the vapor pressure difference.

From the above discussion, it is clear that the effect of salt concentration on the permeation flux is not in the same extent as the temperature effect. This is attributed to the difference in their effects on the driving force of water permeation (vapor pressure). For example, the vapor pressure of the sea water at 60°C is approximately 0.18 bar, whereas it is approximately 0.2 bar for pure water at 60°C and the corresponding vapor pressure of approximately 0.02 bar for both sea and pure water at 20°C.[17,21,46]

Effects of feed and permeate flow rate

The increase of feed and permeate flow velocity played an important role on the membrane permeate flux. This is due to increasing the heat and mass transfer coefficients in the boundary layer near the membrane surface in feed and permeate sides. The membrane surface temperatures were

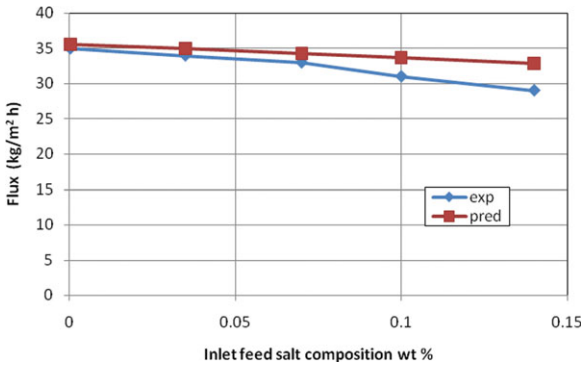

Figure 10. Effect of salt concentration on permeate flux of PP membrane.[46]

[Color figure can be viewed in the online issue, which is available at wileyonlinelibrary.com.]

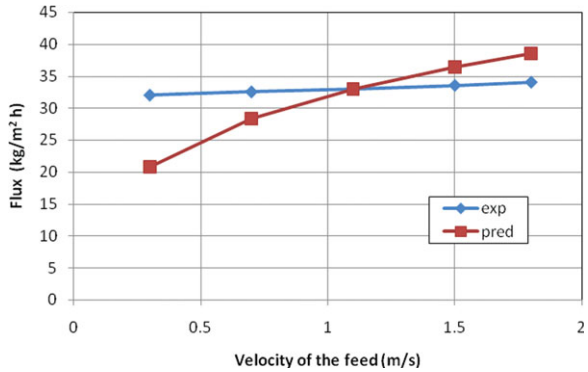

Figure 11. Effect of inlet feed flow rate on permeate flux.[46]

[Color figure can be viewed in the online issue, which is available at wileyonlinelibrary.com.]

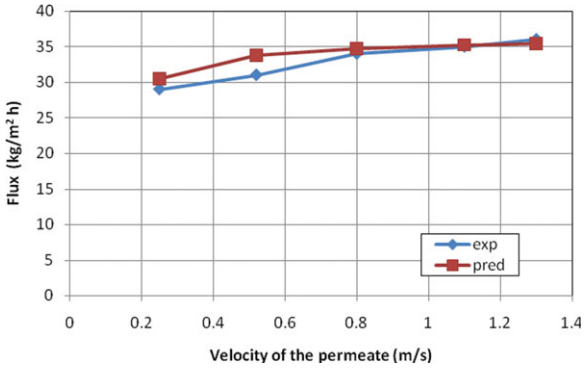

Figure 12. Effect of permeate flow rate on permeate flux.[46]

[Color figure can be viewed in the online issue, which is available at wileyonlinelibrary.com.]

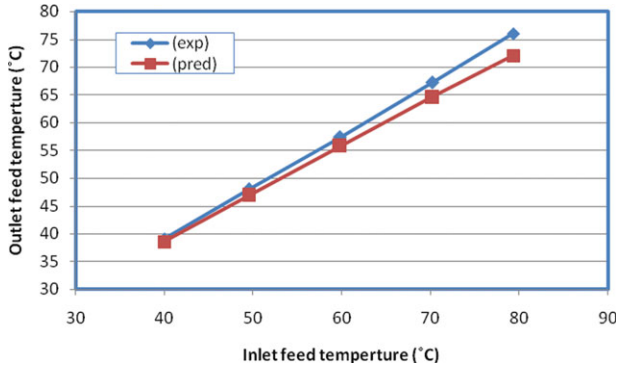

Figure 14. Relationship between the outlet and inlet temperature of the feed stream.[48]

[Color figure can be viewed in the online issue, which is available at wileyonlinelibrary.com.]

brought closer to that of the bulk streams, and the transmembrane temperature difference was thus increased. This led to the reduction of the temperature and concentration polarization effects.

Figures 11 and 12 represent the effects of feed and permeate flow rate on hollow fiber permeate flux. The experimental data of Wang et al.[46] are used to be compared with the results estimated by the presented model. Figure 11 shows that the permeate flux increases when the feed flow rate of NaCl solution is increased. This is due to the fact that with higher flow rate the membrane surface temperatures were brought closer to that of the bulk streams, and the temperature difference was thus increased and led to enhancement of the permeation flux. However, the experimental results gave slightly increase in permeate flux with increase of feed velocity compared with the model results. The comparison between them showed an average deviation of 14%. In fact, from the literature it is found in MD systems that the permeation flux increases with feed velocities and tends to an asymptotic value at higher feed flow rates.[7,52,53]

Figure 12 shows that the permeation flux increases with increasing of the velocity in permeate side. From the predicted results by the presented model, it was found that the average deviation is about 4% from the experimental results. From Figures 11 and 12, it can be concluded that the velocity of the permeate stream estimated by the present model has less effect on the permeation flux than the effect of the velocity of the feed stream. This result is due to the higher temperature polarization in the feed side than that in the permeate side.[54] Banat[55] found that the flow rates of permeate had no effect on the permeation flux, whereas, many literature found that the permeate flux increases with the permeate flow rate.[7,25,56,57] The model results show that at high permeate flow rate there is no significant effect on the permeation flux and this maybe give an explanation for Banat[55] conclusion.

In this study, there are 97 experimental data collected from the literature. These data were, for different membrane types, and membrane characterizations. These data represent the variation of the permeate flux of water across the membrane as a function of feed temperature, salt concentration, flow rate of feed stream or flow rate of permeate stream. These data are used for verifying the validity of the model. Figure 13 shows the performance for the model predictions against all these experimental data.

Temperature prediction by the model

To confirm that the model simulates the operation of DCMD well, the temperature of the outlet streams of feed and permeate predicted by the presented model are compared with that of experimental results reported in the literature.[6,48] Figures 14 and 15 show the outlet feed temperatures verses inlet feed temperatures, while Figure 16 shows the outlet permeate temperatures vs. inlet feed temperatures. The comparison between the results predicted by the model are in a good agreement with the experimental results reported

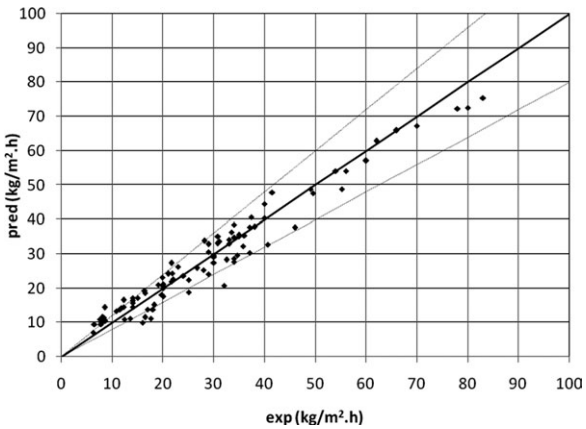

Figure 13. Comparison between the results of the model with experimental data of permeation fluxes via DCMD.

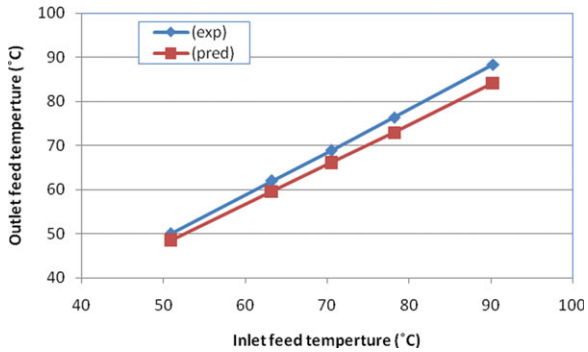

Figure 15. Relationship between the outlet and inlet temperature of the feed stream.[6]

[Color figure can be viewed in the online issue, which is available at wileyonlinelibrary.com.]

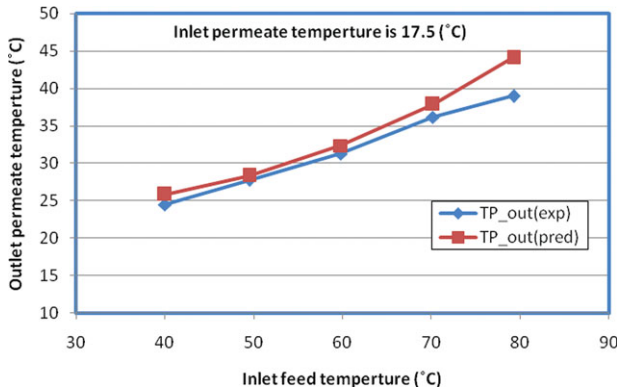

Figure 16. Relationship between the outlet temperature of the permeate stream against inlet temperature of the feed.[6]

[Color figure can be viewed in the online issue, which is available at wileyonlinelibrary.com.]

by Bonyadi et al.[48] and Wang et al.[6] The average deviations between them are about 4, 3, and 6% as shown in Figures 14–16, respectively.

Mean pore size and tortuosity of the membrane

Regarding the characterization of the membrane, Lawson and Lloyd[17] reported that the permeation flux (N) is proportional to the membrane characteristic and can be expressed using the following equation

$$N \propto \frac{r^a \varepsilon}{\delta \tau} \tag{17}$$

where (r) is the mean pore radius of the membrane pores, (a) represents the factor value, which equals to 1 or 2 for Knudsen diffusion and viscous fluxes, (ε) is the membrane porosity, (δ) is the membrane thickness, and (τ) is the membrane tortuosity.

The values of the characterization in Eq. 17 play very important role in accurate evaluation of the permeation flux theoretically. The values of some characterizations of the membrane that appear in Eq. 17 are determined in fair accurately as uniform value such as the membrane thickness and the porosity.

The mechanisms of mass transfer through membrane pores are analyzed in DCMD assuming a uniform pore size of the entire membrane. The pore size distribution of the MD membrane led to more than one mechanism of mass transfer may be occurring simultaneously across the membrane.[43] The pore size distributions were ignored in most modeling studies and considered by the other few literatures.[42,43] Unfortunately most researchers did not report the pore size distribution in their studies. Therefore in this effort, the mean pore size of the membrane is taking into account in the present model. This assumption is maybe one of the expected reasons for the appearing some deviations between the permeation flux predicted by the model and of that of the quoted experimental data.

The membrane pores do not go straight across the membrane and the diffusing molecules must move along tortuous paths, which lead to fluxes decay. In fact, no systematic study had been performed on the effect of tortuosity on MD flux. Most of the theoretical approaches considered the tortuosity as an adjustment parameter helping on the prediction of the MD fluxes. The values of this parameter must be evaluated experimentally, however, due to the difficulties in measuring its real value experimentally for any microporous membrane used in MD process; the investigators frequently assume it.[18] Some studies related the tortuosity with porosity via correlation.[58,59] Khayet and Matsuura[59] stated that "In MD studies the values of 2 is frequently assumed for tortuosity factor to predict MD fluxes although the value 3.9 was reported in the literatures." The values of tortuosity were assumed 1 and near 1 in another literature.[60]

Figure 17 shows the effect of inlet feed temperature at various tortuosity on permeation fluxes predicted by the model comparing with the experimental data of Wang et al.[6] It is clear from this figure that the value of tortuosity plays an important role in the evaluation of permeate fluxes and upgrading the model performance. This figure indicated that as the tortuosity increases from 1.5 to 3, the trend of the permeate flux with the inlet temperature changes from a linear to a nonlinear behavior. This explains the linear trend of the simulated results of the present model appeared in Figures 4, 5, 7. In these figures, the linearity of the simulation results due to the selected values of tortuosity leads to some deviations comparing with the experimental data.

A comparison between the model proposed in this work and models selected from the literature in terms of accuracy is shown as follows: Song et al.,[1] compared the results predicted by the model with experimental results for shell-side feed outlet temperatures, lumen side permeates outlet temperatures, and water permeates flux in hollow fiber DCMD system for water desalination. The model results trend to be underestimated for outlet feed temperatures with a deviation error less than 10% and was able to predict these values well over a temperature range varying between 30 and 90°C. The trend of model to predict the outlet permeate temperature was overpredicted at lower temperatures and underpredicted at higher temperatures with deviation error less than 20% over a temperature range also varying between 30 and 90°C. Moreover, the authors compared the predicted permeate flux with DCMD experimental results and found that the scatter was larger between them and the deviation was less than 20%. Laganà et al.,[25] found that there is a good agreement between the experimental results and their developed model in terms of the effects of feed and permeate flow rate, inlet feed concentration and permeate temperature on the

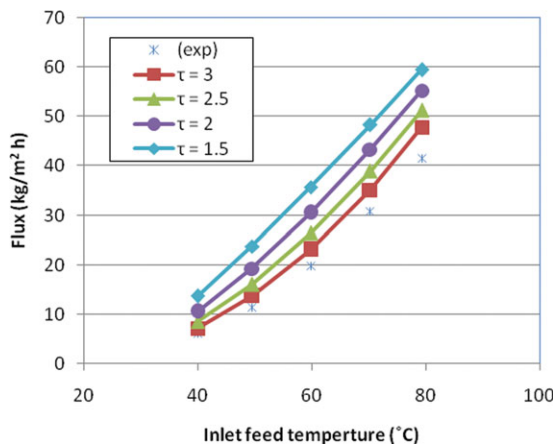

Figure 17. The effect of the inlet feed temperature on the permeation fluxes at various tortuosity predicted by the model with experimental data.[6]

[Color figure can be viewed in the online issue, which is available at wileyonlinelibrary.com.]

permeate flux to produce a concentrated apple juice by using hollow fiber DCMD system. Hwang et al.[61], proposed a two-dimensional model containing mass, energy, and momentum balance for predicting permeate flux for a flat-sheet module via a DCMD system. The modeling results were compared with the experimental results of permeate fluxes from different velocity conditions. For lower inlet feed temperature conditions, modeling results was better than that for higher temperature compared with experimental results. For higher temperature curve, there was underestimation with deviation error less than 10%. The authors also compared the temperature profile for both experiment result and modeling result and they found that the percentage error was less than 5%. Few studies compared the proposed model with experimental data presented in the literature. For example, Close and Sorensen,[21] proposed a mathematical model of DCMD system for water desalination and compared their results with the few experimental data presented in the literature. They found that the permeate fluxes by the developed model as a function of hot feed seawater temperature (from 40 to 70°C) were in excellent agreement with the experimental data. Based on what has been mentioned above, it can be observed that the verification of the proposed model in this work based on wide range of experimental work from the literature is good and there is a reasonable accuracy compared with the models presented in the literature mentioned above.

Conclusions

New simultaneous heat and mass transfer model in DCMD in a hollow fiber configuration is presented in this study. The model of DCMD developed in this work taking into account all aspects of the process, going further than any model previously done by any other researchers in terms of the test of its validity with various membrane polymers, membrane characteristics, module characteristics, and operating conditions. The influence of the temperature and velocity of the feed and permeate streams, and the salt concentration of the feed along the module on the permeate flux are evaluated by the present model and compared with the experimental results collected from the literature. The effect of salt concentration on the permeation flux is not in the same extent as the temperature effect due to the difference in their effects on the driving force of water permeation. The present model is taking into account the mean pore size of the membrane due to the lack information of the pore size distribution in the literature. The model results show that at high permeate flow rate there is no significant effect on the permeation flux. The value of tortuosity could be considered as the tuning values for upgrading the performance of the model. Finally, good agreement is found between the results given by the model and different experimental results presented in the literature.

Notation

Capital letters

A = surface area, m^2
C_T = total concentration, $gmol/m^3$
D = shell diameter, m
D_{AB} = diffusivity, m^2/s
H = enthalpy, kJ/kg
K = membrane distillation coefficient, kg/Pa m^2 s)
L = module length, m
Mwt = molecular weight, g/gmol
N = mass flux, kg/m^2 s
Q = heat flux, W
P^{∇} = vapor pressure, Pa
R = universal gas constant, 8.314 J/gmol.K
T = temperature, °C or K
$\bar{T}$ = average temperature, °C or K
TPC = temperature polarization coefficient

Lowercase letters

h = heat transfer coefficient, W/m^2 K
k = thermal conductivity, W/m K
k = mass transfer coefficient, m/s
k_B = Boltzmann constant, 1.381 J/K
l = cell length, m
m = mass flow rate, kg/s
p = partial pressure, Pa
r = pore radius, m
r_o = external radius, m
r_i = internal radius, m
x = mole fraction

Greek letters

α = activity coefficient
β = membrane permeability, kg/Pa m^2 s
δ = membrane thickness, m
ε = porosity
μ = viscosity, Pa s
ρ = density, kg/m^3
$\lambda_{W\text{-}A}$ = mean molecular free path of water in air, m
σ = collision diameter
τ = tortuosity

Subscripts

A = air
B = in the Bulk
i = cells counter
M = at Membrane surface
ln = Logarithmic mean
ro = based on external radius
ri = based on internal radius
W = water
W = at wall

Superscript

F = Feed side
G = gas
K = Knudson diffusion
L = liquid
M = membrane
MD = Molecular diffusion
P = Permeate side
V = Vapor

Dimensionless numbers used in semiempirical equations

Gz = Graetz No.
Kn = Knudsen No.
Nu = Nusselt No.
Pr = Prandtl No.
Re = Reynolds No.

Literature Cited

1. Song L, Li B, Sirkar KK, Gilron JL. Direct Contact Membrane Distillation-Based Desalination: Novel Membranes, Devices, Larger-Scale Studies, and a Model. *Ind Eng Chem Res*. 2007;46:2307–2323.
2. Shuguang D. Solar desalination of brackish water using membrane distillation process, New Mexico water resources research institute. WRRI Technical Completion Report No. 342. 2008.
3. Khayet M, Godino MP, Mengual JI. Theoretical and experimental studies on desalination using the sweeping gas membrane distillation. *Desalination*. 2003;157:297–305.
4. Bouguecha S, Dhahbi M. Fluidised bed crystalliser and air gap membrane distillation as a solution to geothermal water desalination. *Desalination*. 2003;52:237–244.

5. Ding Z, Liu L, El-Bourawi M, Ma R. Analysis of a solar-powered membrane distillation system. *Desalination.* 2005;172,27–40.
6. Wang KY, Chung TS, Gryta M. Hydrophobic PVDF hollow fiber membranes with narrow pore size distribution and ultra-thin skin for the freshwater production through membrane distillation. *Chem Eng Sci.* 2008;63:2587–2594.
7. Khayet M, Godino MP, Mengual JI. Possibility of nuclear desalination through various membrane distillation configurations: a comparative study. *Int J Nucl Desalinat.* 2003;1:30–46.
8. Khayet M, Mengual JI, Zakrzewska-Trznadel G. Direct contact membrane distillation for nuclear desalination: Part II. Experiments with radioactive solutions. *Int J Nucl Desalinat.* 2006;56:56–73.
9. Duan SH, Ito A, Ohkawa A. Removal of trichloroethylene from water by aeration, pervaporation and membrane distillation. *J Chem Eng Jpn.* 2001;34:1069–1073.
10. Banat FA, Simandl J. Removal of benzene traces from contaminated water by vacuum membrane distillation. *Chem Eng Sci.* 1996;51:1257–1265.
11. Banat FA, Al-Shannag M. Recovery of dilute acetone–butanol–ethanol (ABE) solvents from aqueous solutions via membrane distillation. *Bioprocess Eng.* 2000;23:643–649.
12. Banat FA, Simandl J. Membrane distillation for propane removal fromaqueous streams. *J Chem Technol Biotechnol.* 2000;75:168–178.
13. Garcia-Payo MC, Izquierdo-Gil MA, Fernandez-Pineda C. Air gap membrane distillation of aqueous alcohol solutions. *J Membr Sci.* 2000;169:61–80.
14. Tang JJ, Zhou KG, Zhao FG, Li RX, Zhang QX. Hydrochloric acid recovery from rare earth chloride solutions by vacuum membrane distillation (1) Study on the possibility. *J Rare Earths.* 2003;21:78–82.
15. Alkhudhiri A, Darwish N, Hilal N. Membrane distillation: a comprehensive review. *Desalination.* 2012;287:2–18.
16. Khayet M, Godino MP, Mengual JI. Study of asymmetric polarization in direct contact membrane distillation. *Sep Sci Technol.* 2004;39:125–147.
17. Lawson KW, Lloyd DR. Review Membrane distillation. *J Membr Sci.* 1997;124:1–25.
18. El-Bourawi MS, Ding Z, Ma R, Khayet M. A framework for better understanding membrane distillation separation process. *J Membr Sci.* 2006;285:4–29.
19. Qtaishat M, Matsuura T, Kruczek B, Khayet M. Heat and mass transfer analysis in direct contact membrane distillation. *Desalination.* 2008;219:272–292.
20. Bui VA, Vu LTT, Nguyen MH. Modelling the simultaneous heat and mass transfer of direct contact membrane distillation in hollow fiber modules. *J Membr Sci.* 2010;353:85–93.
21. Close E, Sørensen E. Modelling of Direct Contact Membrane Distillation for Desalination. 20th European Symposium on Computer Aided Process Engineering- ESCAPE20S, 2010 Elsevier B.V
22. Phattaranawik J, Jiraratananon R, Fane AG. Heat transport and membrane distillation coefficients in direct contact membrane distillation. *J Membr Sci.* 2003;212:177–193.
23. Teoh MM, Bonyadi S, Chung TS. Investigation of different hollow fibers module designs for flux enhancement in the membrane distillation process. *J Membr Sci.* 2008;311:371–379.
24. Bird RB, Stewart WE, Lightfoot EN. *Transport Phenomena*, 1st ed. New York: Wiley, 1960.
25. Laganà F, Barbieri G, Drioli E. Direct contact membrane distillation: modeling and concentration experiments. *J Membr Sci.* 2000;166:1–11.
26. Lawson KW, Lloyd DR. Membrane Distillation. II. Direct contact MD. *J Membr Sci.* 1996;120:123–133.
27. Sieder E.N, Tate G.E. Heat transfer and pressure drop of liquid in tubes. *Ind Eng Chem.* 1936;28:1429–1435.
28. Gryta M, Tomaszewska M. Heat transport in membrane distillation process, *J Membr Sci.* 1998;144:211–222.
29. Gryta M, Tomaszewska M, Morawski AW. Membrane distillation with laminar flow. *Sep Purif Technol.* 1997;11:93–101.
30. Thomas LC. *Heat Transfer*, 2nd ed. Englewood Cliffs NJ: Prentice-Hall, 1992.
31. Mengual JI, Khayet M, Godino MP. Heat and mass transfer in vacuum membrane distillation. *Int J Heat Mass Trans.* 2004;47:865–875.
32. Hagan KP. *Heat Transfer with Application.* Englewood Cliffs, NJ: Prentice-Hall, 1990.
33. Dittus FW, Boelter LMK. *Publications on Engineering*, Vol.2. Berkeley: University of California, 1930.
34. Ozisik MN. *Heat Transfer: A Basic Approach.* New York: McGraw-Hill., 1985.
35. Aravinth S. Prediction of heat and mass transfer for fully developed turbulent fluid flow through tubes. *Int J Heat Mass Transfer.* 2000;43:1399–1408.
36. Imdakm AO, Matsuura T. Simulation of heat and mass transfer in direct contact membrane distillation (MD): the effect of membrane physical properties. *J Membr Sci.* 2005;262:117–128.
37. Ozisik MN. *Heat Transfer: A Basic Approach.* Singapore: McGraw-Hill, 1985.
38. White FM. *Heat and Mass Transfer*. USA: Addison-Wesley Publishing Company, Inc., 1991.
39. McCabe WL, Smith JC, Harriott P. *Unit Operations of Chemical Engineering*, 4th ed. New York: McGraw-Hill, 1985.
40. Teoh MM, Chung TS. Membrane distillation with hydrophobic macrovoid-free PVDF–PTFE hollow fiber membranes. *Sep Purif Technol.* 2009;66:229–236.
41. Qtaishat MR. Use of vacuum membrane distillation for concentrating sugars and dyes from their aqueous solutions. MSc Thesis. Jordan University of Science and Technology. Jordan., 2004.
42. Phattaranawik J, Jiraratananon R, Fane AG. Effect of pore size distribution and air flux on mass transport in direct contact membrane distillation. *J Membr Sci.* 2003;215:75–85.
43. Khayet M, Velazquez A, Mengual JI. Modeling of mass transport through a porous partition: Effect of pore size distribution. *Non-Equilib Thermodyn.* 2004;29:279–299.
44. Kuhn H, Fostering HD. *Principles of Physical Chemistry*, 1st ed. New York: Wiley, 2000.
45. Cussler EL. *Diffusion, Mass Transfer in Fluid System*, 2nd ed. New York: Cambridge University Press, 1997.
46. Wang KY, Foo SW, Chung TS. Mixed matrix PVDF hollow fiber membranes with nanoscale pores for desalination through direct contact membrane distillation. *Ind Eng Chem Res.* 2009;48:4474–4483.
47. Lei Z, Chen B, Ding Z. *Special Distillation Processes*, 1st ed. Amsterdam: Elsevier, 2005.
48. Bonyadi S, Chung TS. Flux enhancement in membrane distillation by fabrication of dual layer hydrophilic–hydrophobic hollow fiber membranes. *J Membr Sci.* 2007;306:134–146.
49. Gryta M. Influence of polypropylene membrane surface porosity on the performance of membrane distillation process. *J Membr Sci.* 2007;287:67–78.
50. Chung TS, Jiang LY, Li Y, Kulprathipanj S. Mixed matrix membranes (MMMs) comprising organic polymers with dispersed inorganic fillers for gas separation. *Prog Polym Sci.* 2007;32:483–507.
51. Gryta M, Tomaszewska M, Grzechulska J, Morawski AW. Membrane distillation of NaCl solution containing natural organic matter. *J Membr Sci.* 2001;181:279–287.
52. Banat FA, Simandl J. Theoretical and experimental study in membrane distillation. *Desalination.* 1994;95:39–52.
53. Alkaibi AM, Lior N. Membrane distillation desalination: Status and potential. *Desalination.* 2004;171:111–131.
54. Khayet M, Godino MP, Mengual JI. Thermal boundary layers in sweeping gas membrane distillation. *AIChE J.* 2002;48:1488–1497.
55. Banat FA. Membrane distillation for desalination and removal of volatile organic compounds from water. PhD thesis. McGill University. Canada, 1994.
56. Khayet M, Mengual JI, Matsuura T. Porous hydrophobic/hydrophilic composite membranes: application in desalination using direct contact membrane distillation. *J Membr Sci.* 2005;252:101–113.
57. Ohta K, Kikuchi K, Hayano I, Okabe T, Goto T, Kimura S, Ohya H. Experiments on sea water desalination by membrane distillation. *Desalination.* 1990;78:177–185.
58. Srisurichan S, Jiraratananon R, Fane AG. Mass transfer mechanisms and transport resistances in direct contact membrane distillation process. *J Membr Sci.* 2006;277:186–194.
59. Khayet MS, Matsuura T. *Membrane Distillation: Principles and Applications*, 1st ed. Amsterdam: Elsevier, 2010.
60. Zhang J. Theoretical and experimental investigation of membrane distillation. PhD Thesis; Australia: Victoria University, 2011.
61. Hwang,HJ, He K, Gray S, Zhang J, Moon IS. Direct contact membrane distillation (DCMD): experimental study on the commercial PTFE membrane and modeling. *J Membr Sci.* 2011;371:90–98.

Manuscript received Dec. 4, 2011, and revision received Apr. 21, 2012.

View publication stats